Three-dimensional stability of a vortex pair

Paul Billant
LadHyX, CNRS-UMR 7646, École Polytechnique, F-91128 Palaiseau Cedex, France and Météo-France CNRM Toulouse, 42 Avenue Coriolis, F-31057 Toulouse, France

Pierre Brancher and Jean-Marc Chomaz
LadHyX, CNRS-UMR 7646, École Polytechnique, F-91128 Palaiseau Cedex, France

(Received 1 December 1998; accepted 29 April 1999)

This paper investigates the three-dimensional stability of the Lamb–Chaplygin vortex pair. Short-wavelength instabilities, both symmetric and antisymmetric, are found. The antisymmetric mode possesses the largest growth rate and is indeed the one reported in a recent experimental study [J. Fluid Mech. **360**, 85 (1998)]. The growth rates, wave numbers of maximum amplification, and spatial eigenmodes of these short-wavelength instabilities are in good agreement with the predictions from elliptic instability theory. A long-wavelength symmetric instability similar to the Crow instability of a pair of vortex filaments is also recovered. Oscillatory bulging instabilities, both symmetric and antisymmetric, are identified albeit their growth rates are lower than for the short-wavelength instabilities. Their behavior and eigenmodes resemble those of the oscillatory bulging instability occurring in the mixing layer. © *1999 American Institute of Physics.* [S1070-6631(99)04008-8]

I. INTRODUCTION

A vortex pair consists of two counter-rotating vortices propagating steadily, one vortex being translated under the velocity field of the other. The three-dimensional stability of such flow is of interest for the understanding of coherent structure dynamics and within the aeronautical context. Indeed, vortex pairs form at the trailing edges of airplane wings and may perturb airplanes that follow behind. Such hazard limits maximum take-off and landing cadences in airports.

Many theoretical stability studies have been devoted to the vortex pair or to related configurations, beginning with the investigation of Crow[1] of a pair of counter-rotating vortex filaments. Crow has discovered a long-wavelength instability consisting of a sinusoidal symmetric (with respect to the middle plane between the vortices) deformation of the vortices. In addition, he found both symmetric and antisymmetric short-wavelength instabilities. These short-wavelength instabilities were shown to be spurious by Widnall, Bliss, and Tsai[2] because at such small scale, a finite-core vortex can no longer be modeled by a vortex filament. However, this led Widnall *et al.*[2] to realize that another type of short-wavelength instability could exist, initiating a large body of work.[3–7] In these fundamental studies, only a single vortex was considered, the influence of the other being modeled by the presence of a strain under which the streamlines become elliptical. These studies, either asymptotic for small strain[3,4,6] or numerical[5,7] have shown the existence of short-wavelength bending instabilities with increasing complex radial structure as the axial wave number is increased. The physical mechanism is a resonant interaction between the strain and Kelvin waves with azimuthal wave numbers $m=1$ and $m=-1$ when both waves have the same frequency. Such a mechanism is identical to the one underlying the elliptic instability of unbounded vortices discovered later.[8–10] The only difference between unbounded and confined vortices is that the continuous instability wave number band is discretized by the finite size of the core into an infinite number of separate instability curves.

In the case of the vortex pair, it is only recently that careful experiments have been able to reveal the occurrence of the short-wavelength instability.[11–13] In particular, Leweke and Williamson[12] have shown that the antisymmetric configuration is selected. Since no stability analysis of finite-core vortex pair exists, the experimental results have been compared to theoretical studies of idealized single elliptical vortices with uniform vorticity. However, the streamlines in a vortex pair are not exactly elliptical and the vorticity is not uniform so that it is unclear to which extent quantitative comparisons are relevant. Furthermore, because only one vortex is studied, these theoretical investigations are unable to explain the selection between antisymmetric and symmetric modes. A similar situation prevails regarding the long-wavelength Crow instability; the quantitative results for the pair of vortex filaments are the only basis to which experimental results are compared,[11,14,15] although this asymptotic formulation is restricted to long axial wavelength disturbances and well-separated vortices.

This bears testimony for the need of a stability analysis of a realistic vortex pair configuration. In this paper, we shall present the three-dimensional stability analysis of the Lamb–Chaplygin vortex pair.[16–19] This steady flow, which is presented in Sec. II A, is an exact solution of the Euler equations. In Secs. II B and II C, we give the linearized equations and outline the numerical method. In Sec. III, the results of the computations are discussed.

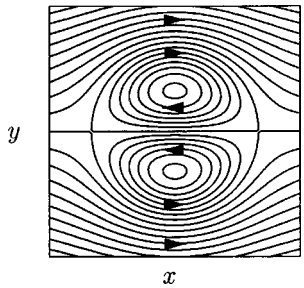

FIG. 1. Streamlines of the Lamb–Chaplygin vortex pair.

II. FORMULATION

In what follows, we use either Cartesian coordinates (x,y,z), with z along the dipole axis or cylindrical coordinates (r,θ,z) with $x=r\cos\theta$ and $y=r\sin\theta$.

A. Lamb–Chaplygin's vortex pair

The Lamb–Chaplygin dipole[16–19] is chosen as a basic state. This exact solution of the incompressible Euler equations describe a pair of counter-rotating vortices. The explicit stream function ψ_0 and axial vorticity $\omega_{z0}=\Delta\psi_0$ of this solution expressed in a comoving frame of reference are

$$\left.\begin{aligned}\psi_0(r,\theta)&=-\frac{2UR}{\mu_1 J_0(\mu_1)}J_1\left(\mu_1\frac{r}{R}\right)\sin\theta,\\ \omega_{z0}&=-\frac{\mu_1^2}{R^2}\psi_0,\end{aligned}\right\}\quad r\leqslant R, \tag{1}$$

$$\left.\begin{aligned}\psi_0(r,\theta)&=-Ur\left(1-\frac{R^2}{r^2}\right)\sin\theta,\\ \omega_{z0}&=0,\end{aligned}\right\}\quad r>R, \tag{2}$$

where U is the propagating velocity of the dipole, R its radius, J_0 and J_1 are the Bessel functions of zero and first order, and $\mu_1=3.8317$ is the first zero of J_1. The associated horizontal velocity is given by $\mathbf{u}_0=-\boldsymbol{\nabla}\times(\psi_0\mathbf{e}_z)$, where $\mathbf{e}_z$ is the unit vector in the axial direction.

The streamlines of the Lamb–Chaplygin vortex pair are shown in Fig. 1. Such basic flow has provided a good theoretical model for dipoles generated by various means in laboratory studies.[20–22] In the present context, it is noteworthy that the Lamb–Chaplygin vortex pair shows a strong resemblance to the vortex pair produced by a flap mechanism in the recent experimental investigation of short-wavelength instabilities by Leweke and Williamson.[12]

B. Linearized equations

The two-dimensional basic states (1)–(2) are subjected to infinitesimal three-dimensional perturbations governed by the nondimensional linearized equations for the perturbation velocity $\tilde{\mathbf{u}}$, vorticity $\tilde{\boldsymbol{\omega}}=\boldsymbol{\nabla}\times\tilde{\mathbf{u}}$ and pressure $\tilde{p}$,

$$\frac{\partial\tilde{\mathbf{u}}}{\partial t}+\omega_{z0}\mathbf{e}_z\times\tilde{\mathbf{u}}+\tilde{\boldsymbol{\omega}}\times\mathbf{u}_0=-\boldsymbol{\nabla}(\tilde{p}+\mathbf{u}_0\cdot\tilde{\mathbf{u}})+\frac{1}{\mathrm{Re}}\Delta\tilde{\mathbf{u}}, \tag{3}$$

$$\boldsymbol{\nabla}\cdot\tilde{\mathbf{u}}=0. \tag{4}$$

Space and time have been nondimensionalized by the dipole radius R and the time scale R/U. Then, the Reynolds number Re is defined as $\mathrm{Re}=UR/\nu$, where ν is the kinematic viscosity. The viscous diffusion of the basic state is omitted as classically done in viscous stability analysis.[23] This reasonably describes the dynamics of a real flow if the growth rate of three-dimensional instabilities is large compared to the viscous damping of the basic flow. Two Reynolds numbers will be investigated; $\mathrm{Re}=10^4$ which is close to the inviscid limit and $\mathrm{Re}=400$ which corresponds to the Reynolds number of the experimental investigation of Leweke and Williamson[12] (using the present definition of the Reynolds number).

As the basic state is uniform along the z axis, the following normal mode decomposition is imposed on the perturbation

$$[\tilde{\mathbf{u}};\tilde{\boldsymbol{\omega}};\tilde{p}](x,y,z,t)=[\mathbf{u};\boldsymbol{\omega};p](x,y,t)e^{ik_z z}+\text{c.c.}, \tag{5}$$

where k_z is the axial wave number and c.c. denotes the complex conjugate.

C. Numerical procedure

In order to study the three-dimensional stability of the vortex pair, we shall not explicitly determine the matrix operator deriving from (3)–(4) and compute all its eigenvalues as done, for instance, by Pierrehumbert and Widnall.[24] Instead, we shall only calculate the eigenvalue with the largest real part by numerically integrating (3)–(4) with a perturbation of the form (5). The perturbation velocity $\mathbf{u}(x,y,t=0)$, defined in (5), is initialized with a divergence-free white noise. Then, by integrating the linear equations (3)–(4) for a sufficiently long time, the most unstable eigenmode emerges after a transient and becomes entirely dominant whereas the less unstable eigenmodes become negligible.[25,26] Therefore, when $t\to\infty$ the velocity $\mathbf{u}(x,y,t)$ tends to a solution of the form, $\mathbf{A}(x,y)\exp(\sigma t)$, where $\sigma=\sigma_r+i\sigma_i$, σ_r being the temporal growth rate and σ_i the frequency of the most unstable eigenmode. It is thus very easy to retrieve the eigenvalue σ and spatial structure $\mathbf{A}(x,y)$ of the most unstable mode for any k_z.

To integrate numerically (3)–(4) for a given k_z, a pseudospectral scheme has been implemented in Cartesian coordinates with periodic boundary conditions. The code was originally written by Vincent and Meneguzzi[27] and adapted to linear stability analyses by Brancher.[28] This code has been successfully validated in the case of jet[29,30] and Stuart's vortices[28] instabilities. The main steps of the numerical method are outlined below.

Variables on the right-hand side of (5) are expressed in Fourier space by application of the two-dimensional Fourier transform, for example,

$$\hat{\mathbf{u}}(k_x,k_y,t)=\int\int\mathbf{u}(x,y,t)e^{-i(k_x x+k_y y)}dxdy, \tag{6}$$

where k_x and k_y are the horizontal components of the total wave number $\mathbf{k}=(k_x,k_y,k_z)$. The two-dimensional Fourier

transforms are computed using the FFT routine from the Cray Scientific Library SciLib. In spectral space, the governing Eqs. (3)–(4) become

$$\frac{\partial \hat{\mathbf{u}}}{\partial t} = \mathbf{P}(\mathbf{k})[\mathbf{u} \times \omega_{z0}\widehat{\mathbf{e}_z} + \mathbf{u}_0 \times \boldsymbol{\omega}] - \frac{\mathbf{k}^2}{\mathrm{Re}}\hat{\mathbf{u}}. \tag{7}$$

The tensor $\mathbf{P}(\mathbf{k})$ with Cartesian components $P_{ij} \equiv \delta_{ij} - k_i k_j / \mathbf{k}^2$ designates the projection operator on the space of divergence-free fields. We recall that k_z is fixed for a given simulation. The products inside the square brackets in (7) are evaluated in the physical space. Time integration is performed with the second-order finite-difference Adams–Bashforth numerical scheme. The dissipative terms are integrated exactly. The 2/3 rule is used for dealiasing. In all simulations, the periodic square box of size $L=9$ is made up of 256×256 collocation points equally spaced on a Cartesian mesh with $\delta x = \delta y = 0.035$. The time increment is chosen to be $\delta t = 0.0019$ such that the Courant condition $\delta x/\delta t = 18.4 > U_{\max}$ is fulfilled, where $U_{\max}=2.5$ is the maximum basic velocity.

In the case of nonoscillatory instabilities, the growth rate σ_r is retrieved by the formula

$$\sigma_r = \lim_{t\to\infty} \frac{1}{2} \frac{d \ln E}{dt}, \tag{8}$$

where $E = \overline{u_x^2} + \overline{u_y^2} + \overline{u_z^2}$ is the energy perturbation, the overbar denoting spatial integration over the square computational domain. To reach an asymptote in this formula and achieve an accuracy for σ_r of at least three significant figures, an integration time of 19 time units is necessary. In most cases, however, this integration time yields an accuracy of four to five significant figures (when the leading eigenvalue is well separated from the others). The spatial structure of the corresponding eigenmode is simply obtained from the velocity field of the last time step. In the case of oscillatory instabilities, the times where $d\ln(E)/dt$ reaches an extremum are detected to evaluate the period T and consequently the pulsation of the wave, i.e., the imaginary part of the eigenvalue $\sigma_i = 2\pi/T$. Accordingly, (8) is replaced by

$$\sigma_r = \lim_{t\to\infty} \frac{1}{2T} \ln\left(\frac{E(t+T)}{E(t)}\right). \tag{9}$$

Practically, once an eigenmode has been determined for certain parameter values (Re,k_z), the parameter space can be explored by continuation to accelerate the convergence towards the most unstable normal mode. Specifically, instead of using a white noise, a simulation can be initialized by the eigenmode calculated at a previous simulation for slightly different parameters (Re,k_z). This initialization mainly serves to save CPU time but it also allows an instability branch to be followed slightly into a domain of the parameter space where it is no longer the most unstable.

The present numerical method mimics the temporal evolution of a perturbation in a real experiment except that the imposed perturbation has a single axial wave number k_z and the basic state is not allowed to diffuse. Because the nonlinear terms are absent in (3), the exponential growth can occur indefinitely which allows the growth rate to be determined as precisely as desired. The advantage of such method over numerical eigenvalue problems lies in its ease of implementation if one disposes of a three-dimensional pseudospectral code. In practice, to adapt such a code to the present study, the velocity field has been separated into a basic flow and a perturbation field, the nonlinear terms have been switched off, the wave number in the axial direction has been fixed and the three-dimensional FFT routines replaced by two-dimensional ones. One disadvantage of this straightforward but efficient procedure is that only the most unstable mode is accessible. The other less unstable modes could nevertheless be obtained via successive orthogonalizations.[25,26] Another limitation is that such method is relatively CPU time-consuming.

TABLE I. Accuracy check of the computed growth rate for $k_z=4$ and $\mathrm{Re}=10^4$. The superscript indicates the number of collocation points.

$\delta x \backslash L$	9	18
0.035	1.220 663[a]	1.220 666[b]
0.018	1.221 477[b]	

[a] 256×256.
[b] 512×512.

The accuracy of the computations has been tested by doubling either the resolution or the box size. Table I shows a typical case for $k_z=4$ and $\mathrm{Re}=10^4$. There is a relative variation of 0.07% of the growth rate when the mesh size is halved and of 0.0002% when the box size is doubled. Such tests have been regularly carried out in order to control the respective influences of the grid discretization and the periodic boundary conditions.

III. RESULTS

The normal modes separate into two classes with distinct symmetries in the y direction: antisymmetric modes whose velocity $\mathbf{u}$ and vorticity $\boldsymbol{\omega}$ fields verify the following symmetries:

$$\begin{aligned} &[u_x, u_y, u_z](x,y) = [-u_x, u_y, -u_z](x,-y), \\ &[\omega_x, \omega_y, \omega_z](x,y) = [\omega_x, -\omega_y, \omega_z](x,-y), \end{aligned} \tag{10}$$

and symmetric modes with the inverse symmetries

$$\begin{aligned} &[u_x, u_y, u_z](x,y) = [u_x, -u_y, u_z](x,-y), \\ &[\omega_x, \omega_y, \omega_z](x,y) = [-\omega_x, \omega_y, -\omega_z](x,-y). \end{aligned} \tag{11}$$

This separation among normal modes arises because the basic state (1)–(2) has the symmetries (11). More physically, antisymmetric and symmetric modes correspond to antisymmetric and symmetric distortions of the two vortices of the pair. In order to retrieve the most unstable modes belonging to each of these two classes, the symmetries (10) and (11) have been successively imposed to the perturbation in two separate sets of numerical simulations. Note that when no symmetry is imposed on the perturbation, the most unstable mode appears to be antisymmetric for most axial wave numbers k_z. We first describe the antisymmetric modes, the symmetric modes being presented in the next section.

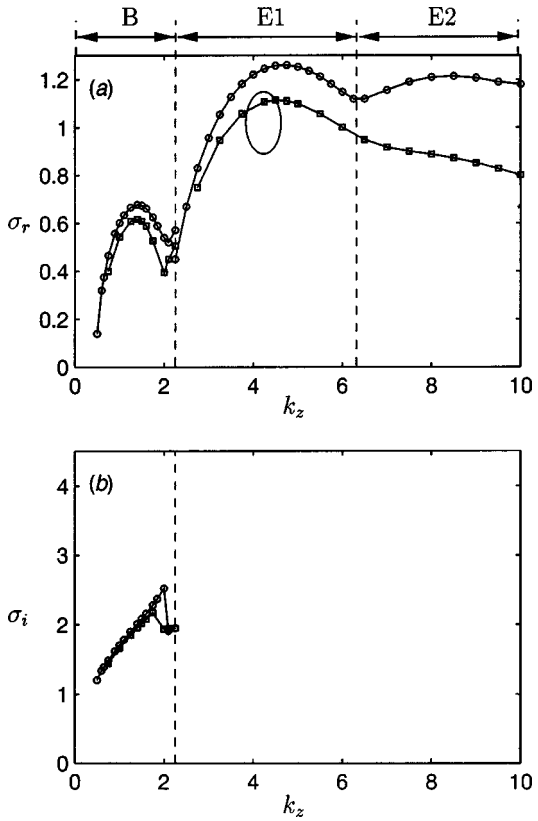

FIG. 2. Nondimensional growth rate σ_r (a) and frequency σ_i (b) of antisymmetric modes as a function of non-dimensional axial wave number k_z for Re$=10^4$ (circle) and Re$=400$ (square). Only nonzero frequencies σ_i are shown. In (a), the large ellipse indicates the experimental measurement of Leweke and Williamson (Ref. 12) for Re$=400$.

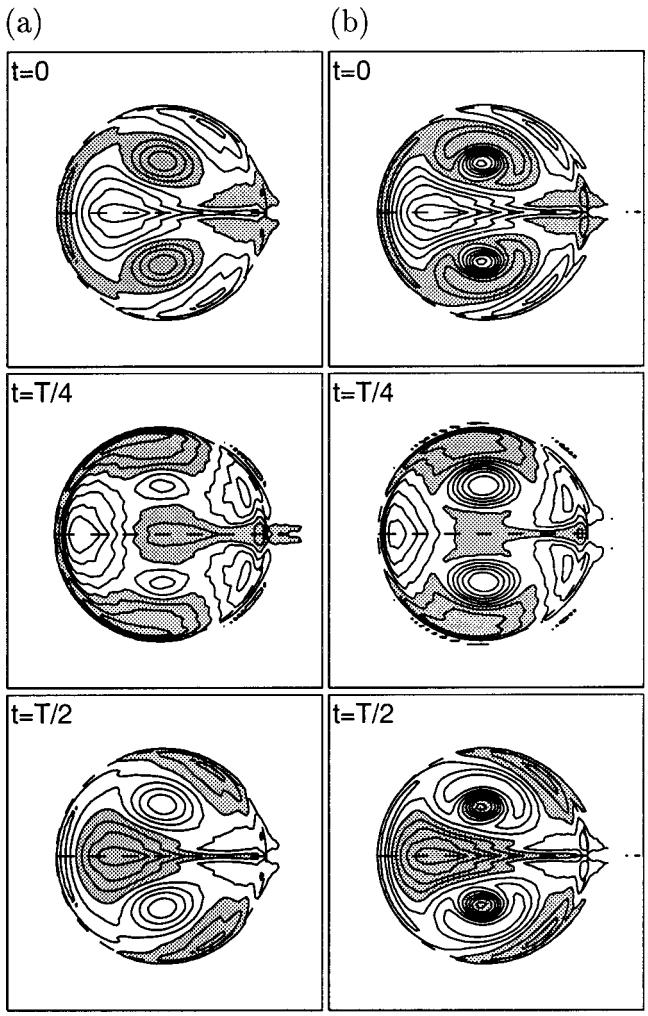

FIG. 3. Contours of axial vorticity of standing oscillatory antisymmetric modes (band B in Fig. 2) in the horizontal plane at three phases of the oscillation cycle $t=0$, $T/4$, $T/2$ at $k_z=1.4$ (a) and $k_z=2.25$ (b) for Re $=10^4$. Only a domain of size 3×3 is shown while the computational domain is 9×9. Shaded areas are regions of negative values. The dashed circle indicates the boundary $r=1$ of the dipole. The dashed line represents the middle plane between the two vortices of the pair. The basic flow is from left to right at infinity. Note that the small distortions seen on some contours in (a) at $t=T/4$ disappear if a 512×512 resolution is used, but the growth rate remains unchanged.

A. Antisymmetric modes

Figure 2(a) shows the nondimensional growth rate σ_r of antisymmetric modes as a function of the nondimensional axial wave number k_z for Re$=10^4$ and Re$=400$. We recall that the corresponding dimensional eigenvalue $\hat{\sigma}$ and axial wave number $\hat{k}_z$ are given by $\hat{\sigma}=\sigma U/R$ and $\hat{k}_z=k_z/R$. In the following discussion, we focus on the stability curves obtained for the Reynolds number Re$=10^4$. The case Re $=400$ is similar except that the growth rate is lowered by viscous effects. These latter results will allow a comparison with experimental results. Three instability bands labeled B, E1, and E2 with respective maxima at the wave numbers $k_z=1.4$, $k_z=4.75$, and $k_z=8.5$ can be seen. In the first band, the instability is oscillatory with a frequency σ_i shown in Fig. 2(b). The axial vorticity ω_z fields of the eigenmode corresponding to these three maxima are displayed in Figs. 3(a) and 4(a)–4(b), respectively. In each case, the axial vorticity component ω_z is symmetric in y as implied by the symmetry (10). The perturbation vorticity is zero outside the circle $r=R$ because the basic flow (1)–(2) is potential there.

Since the first band of instability is oscillatory, the modal structure varies during the oscillation period. Three oscillation phases are shown in Fig. 3(a). The oscillation cycle consists mainly of an appearance/disappearance of the two perturbation vortex cores located in the center of each vortex of the pair. The perturbation is dominated by an azimuthal wave number $m=0$ in the vortex cores and $m=2$ at the periphery [Fig. 3(a)]. Thus, this instability will be characterized by a standing oscillatory π-out-of-phase bulging of each vortex core. Such instability bears a striking resemblance to the ''core dynamic instability'' found by Schoppa, Hussain, and Metcalfe[31] in Stuart mixing layer and which manifests also by a standing oscillation of vortex core size (see also Ref. 32). Moreover, there is a close similarity between the axial vorticity eigenmode in each vortex of the pair [Fig. 3(a)] and the one presented by Schoppa *et al.* [Fig. 10(c) of 31]. For the higher wave numbers near $k_z=2.25$, an interesting feature of this oscillatory instability is that the growth rate σ_r continuously reincreases after a minimum [Fig. 2(a)]. There is a corresponding jump of the frequency σ_i [Fig. 2(b)]. This indicates the presence of a second type of oscillatory instability. The related axial vorticity eigenmode at

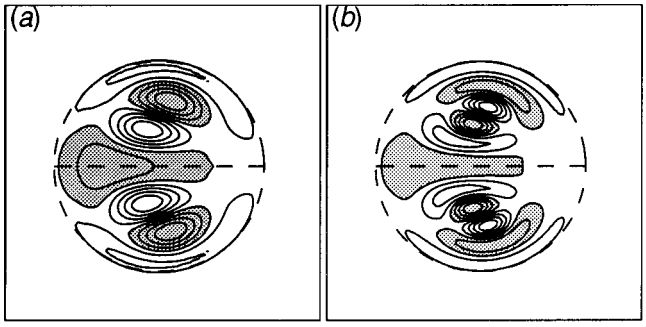

FIG. 4. Contours of axial vorticity of short-wavelength antisymmetric modes in the horizontal plane in the band $E1$ at $k_z=4.75$ (a) and in the band $E2$ at $k_z=8.5$ (b). Same legend as in Fig. 3.

three phases of the oscillation cycle is shown in Fig. 3(b). As in Fig. 3(a), the perturbation in each vortex of the pair is again mostly made of $m=0$ and $|m|=2$ azimuthal modes but now exhibits a more complex radial structure; one radial node line is added in the axial vorticity perturbation [Fig. 3(b)]. However, this second mode of bulging instability is masked at higher wave number by a more unstable nonoscillatory instability (E1).

The eigenmode related to this nonoscillatory instability [band E1 in Fig. 2(a)] is displayed in Fig. 4(a). The perturbation consists of a dipole nested inside each vortex core of the basic state. This corresponds to a dominant azimuthal wave number $|m|=1$ within each vortex core. If this perturbation were superposed to the basic state, it would be seen that such an instability distorts the inner part of each vortex of the pair; the upper vortex core is shifted up and to the left while the lower one is shifted up and to the right. The outer parts of the core are moving in the opposite directions. The numerically computed eigenfunction of Fig. 4(a) resembles closely to the experimental short-wavelength perturbation field measured by Leweke and Williamson [Fig. 10(b) of Ref. 12] on a vortex pair generated by a flap mechanism. This agreement can be further reinforced by comparing the experimentally measured wavelength and growth rate to those of the most amplified disturbance determined in the present investigation. Leweke and Williamson[12] have fitted their vortex pair to two Lamb–Oseen vortices separated of a distance b and with azimuthal velocity $u_\theta=\Gamma/2\pi r(1-\exp -(r/a)^2)$, where Γ is the total circulation of each vortex and a the vortex core size. In terms of these parameters, the experimental dimensional wavelength and growth rate given in Ref. 12 are $\hat{\lambda}=(4\pm0.4)a$ and $\hat{\sigma}_r=(0.94\pm0.12)\Gamma/2\pi b^2$. In the present case, the dimensional Lamb–Chaplygin vortex pair can be also extremely well fitted to two Lamb–Oseen vortices with parameters $\Gamma=2\pi UR$, $b=0.96R$ and $a=0.37R$. Thus, the numerically calculated most amplified wave number and growth rate, $k_z=4.5$ and $\sigma_r=1.11$, for the Reynolds number $\mathrm{Re}=400$ used in the experiment become in terms of these parameters, $\hat{\lambda}=3.77a$ and $\hat{\sigma}_r=1.02\Gamma/2\pi b^2$. The agreement with the experimental wavelength and growth rate is very good. This agreement can be also appreciated from Fig. 2(a), where the experimental measurements converted to our units, i.e., $k_z=4.24\pm0.4$ and $\sigma_r=1.02\pm0.13$, are represented by an ellipse. However, if the wavelength is expressed in term of the vortex separation, Leweke and Williamson[12] report that $\hat{\lambda}=0.77b$, while here we have $\hat{\lambda}=1.45b$. This disagreement results from the difference in core concentration between the Lamb–Chaplygin vortex pair where $a/b=0.39$ and the experimental vortex pair for which $a/b=0.2$. The fact that the experimental and numerical wavelengths agree when expressed in term of the vortex core size and not in term of the vortex separation indicates that the elliptic instability scales indeed on the vortex core size.

The modal axial vorticity [Fig. 4(b)] corresponding to the third growth rate maximum [band $E2$ in Fig. 2(a)] is again made of $|m|=1$ azimuthal modes but with one additional radial node line in each vortex of the basic state. This mode has a slightly lower growth rate than the previous one and in addition is more dampened by viscous effects for $\mathrm{Re}=400$ [Fig. 2(a)].

Leweke and Williamson[12] suggests that this short-wavelength antisymmetric instability ($E1$ and $E2$), which they call ''cooperative elliptic instability,'' is related to the elliptic instability. We shall give further evidences supporting this view. The first indication is the close resemblance of the eigenmode inside each vortex of the pair [Fig. 4(a)] to those obtained for an unbounded elliptical vortex by Pierrehumbert,[8] Baily,[9] and Waleffe.[10] As predicted by the elliptic instability theory, the perturbation in each vortex is tilted relative to the ellipse [Figs. 4(a)–4(b)]. The line joining the vorticity extrema is approximately aligned with the stretching direction which is at 45° and $-45°$ with respect to the x axis for the upper and lower vortex, respectively.[10] The increase of the radial complexity of the perturbation as the wave number increases is also reminiscent of the elliptic instability of a confined vortex (see for instance Fig. 2 of Miyazaki, Imai, and Fukumoto[7]). More quantitative comparisons can be made from the growth rates predicted either by elliptic instability theory for an unbounded vortex[8–10] or for a confined vortex embedded in a strain field.[3–5,7] In the first case, the maximum growth rate σ_r is independent of the axial wave number and proportional to the strain rate ϵ by $\sigma_r=9/16\epsilon=0.5625\epsilon$ for asymptotically small strain rates (small by comparison with the vorticity). In the second case, the confinement through appropriate boundary conditions is found to discretize the wave number band and select eigenmodes with increasing internal radial nodes as the wave number is increased. However, the maximum rate of growth seems to be almost not affected by the confinement. For a slightly elliptic Rankine vortex (straight circular vortex with constant vorticity), Tsai and Widnall[4] found $\sigma_r=0.5708\epsilon$ for the mode with one internal radial node and $\sigma_r=0.5695\epsilon$ for the one with two nodes. These results have been shown to hold quite satisfactorily even for finite strain in the numerical study of Robinson and Saffman[5] of the Moore–Saffman vortex (elliptic uniform patch of vorticity embedded within a strain field). The independence of the maximum growth rate with respect to the internal radial structure of the eigenmode is also a feature observed in Kirchhoff's elliptic vortex[7] (elliptic uniform patch of vorticity without strain field). To compare these results with the present instability, we esti-

mate the strain rate by expanding the basic stream function (1) near one vortex center ($r_c=\mu_m/\mu_1, \theta_c=\pi/2$) of the pair ($\mu_m=1.8412$ is the value at which the Bessel function J_1 is maximum in the interval $[0,\mu_1]$),

$$\psi_0=\frac{1}{2}\left[(\nu-\epsilon)x^2+(\nu+\epsilon)\left(y-\frac{\mu_m}{\mu_1}\right)^2\right] +O\left(x^3,\left(y-\frac{\mu_m}{\mu_1}\right)^3,\ldots\right), \quad (12)$$

where $2\nu=\omega_{0z}(r_c,\theta_c)=2\mu_1 J_1(\mu_m)/J_0(\mu_1)=-11.12$ is the axial vorticity at the vortex center and

$$\epsilon=\mu_1\frac{J_1(\mu_m)}{J_0(\mu_1)}\left(\frac{2}{\mu_m^2}-1\right)=2.28,$$

is the local strain rate. Hence we have the following estimate for the growth rate of the first two modes, $\sigma_r\approx 1.30$ according to Tsai and Widnall[4] or $\sigma_r\approx 1.28$ if we use the relation given by unbounded elliptic instability theory. These values are reasonably close to the value $\sigma_r=1.26$ for the first maximum and $\sigma_r=1.21$ for the second one for $\mathrm{Re}=10^4$ in Fig. 2(a).

We now compare qualitatively the spatial structure of the eigenmodes [Figs. 4(a)–4(b)] to those predicted by Tsai and Widnall[4] for a Rankine vortex in a weak strain field. In the latter case, the axial vorticity has a radial dependence of the form $J_1(\kappa r^*)$ inside the vortical core, where $\kappa=\sqrt{3}k_z$ and r^* is the radius measured from the vortex center. Tsai and Widnall[4] have shown that the first two bands of instability with one and two internal radial nodes have a maximum growth rate for the wave numbers $k_{z1}=2.5/a_r$ and $k_{z2}=4.35/a_r$, respectively, where a_r is the vortex radius. Physically, these wave numbers are those for which Kelvin waves $m=\pm 1$ are steady and can diverge with strain. We therefore deduce that, for $k_z=k_{z1}$, the axial vorticity should have one node in $0<r^*<a_r$ at the radius $r^*=\mu_1/(k_{z1}\sqrt{3})=0.88a_r$ from the center of each vortex of the pair. This compares well with Fig. 4(a) where the axial vorticity reveals one node close to the boundary of each vortex. Similarly, for $k_z=k_{z2}$, the axial vorticity will have two internal radial nodes at $r^*=\mu_1/(k_{z2}\sqrt{3})=0.51a_r$ and $r^*=\mu_2/(k_{z2}\sqrt{3})=0.93a_r$ ($\mu_2=7.0156$ is the second zero of J_1). Indeed, the eigenmode in Fig. 4(b) exhibits two internal nodes at spatial locations not far from these predictions.

The wave numbers at which maximum amplification should occur according to Tsai and Widnall[4] can be also compared to those obtained herein. The main difficulty is that the previous relation for k_{z1} and k_{z2} are defined for a circular vortex with uniform vorticity, while the vortices of the Lamb–Chaplygin dipole are elliptical with distributed vorticity. The effects of these two departures from the theory can be however quantitatively taken into account. With regard to the ellipticity, Robinson and Saffman[5] have shown that when a vortex is fully elliptical, Tsai and Widnall[4] results continue to be valid if the radius a_r is taken as the geometric mean $a_r=(cd)^{1/2}$ of the semimajor c and semiminor d axes of the ellipse. (Note that this result can be justified from the work of Waleffe[10] in the small ellipticity limit.) For the vortices of the pair, the semimajor axis is the dipole radius $c=1$ and the semiminor axis is half a radius $d=0.5$ giving $a_r=\sqrt{0.5}$. In order to take into account the effect of the vorticity distribution, we use the results of Widnall *et al.*[2] for a vortex with distributed vorticity $\omega_z=(r^{*2}-a_d^2)^2$, which approximately represents the vorticity inside the vortices of the Lamb–Chaplygin dipole. In this case, the most amplified wave numbers should be $k_{z1}=3.9/a_d$ and $k_{z2}=7/a_d$. Using the previous estimate for the radius $a_d=a_r=\sqrt{0.5}$, this yields the predictions $k_{z1}\approx 5.5$ and $k_{z2}\approx 9.9$. These wave numbers are close to those calculated in the present study ($k_{z1}=4.75$ and $k_{z2}=8.5$ for $\mathrm{Re}=10^4$).

The present results can be also tested against elliptic instability theory for unbounded vortices. However, as a consequence of the absence of outer boundary conditions, there is no particular axial wave number more amplified than the others. Thus, similar predictions to those given above can not be obtained within the frame of elliptic instability theory. Nonetheless, it is possible to make a self-consistency check between the spatial structure of the eigenmodes shown in Figs. 4(a)–4(b) and the wave numbers at which they are observed. To this end, we shall use the results of Waleffe[10] which are valid for finite strain. As in Tsai and Widnall,[4] the radial dependence of the axial vorticity is $J_1(\kappa r^*)$, but now r^* is defined from elliptico-polar coordinates, $x=r^*E\cos\theta$, $y=r^*\sin\theta$, where $E=c/d$ is the aspect ratio of the elliptical streamlines. In the vortex cores of the pair, the aspect ratio is $E=\sqrt{(\nu+\epsilon)/(\nu-\epsilon)}\approx 1.55$ from (12). The coefficient κ is related to the latter aspect ratio by $\kappa=k_zE\tan\alpha$ where α is the angle between the wave vector and the rotation axis. The dependence of α with E at maximum growth rate is not provided by Waleffe,[10] however this information can be found in Baily,[9] $\alpha\approx 0.3\pi$. We measure next that the first radial node is at $r^*\approx 0.34$ in Fig. 4(a) and at $r^*\approx 0.21$ in Fig. 4(b). This yields the predictions $k_{z1}=\mu_1/(r^*E\tan\alpha)\approx 5.3$ and $k_{z2}\approx 8.6$ which are in good agreement with the location of maxima in Fig. 2(a).

B. Symmetric modes

The growth rate of symmetric modes is shown in Fig. 5 for $\mathrm{Re}=10^4$ and $\mathrm{Re}=400$. Again, we shall discuss mainly the results for $\mathrm{Re}=10^4$, the growth rate curves for $\mathrm{Re}=400$ being similar. There are four instability bands labeled C, B, $E1$ and $E2$. Also shown is the long-wavelength symmetric instability mode as predicted by Crow's theory for a pair of vortex filaments propagating at the same speed and separated by a distance $b=0.96$, which is the distance between vortex centers in the Lamb–Chaplygin vortex pair. This Biot–Savart cutoff theory requires also the effective core size a_e of the vortices. The concept of effective core size which has been introduced by Widnall, Bliss, and Zalay[33,34] (see also a more recent derivation by Klein and Knio[35]), states that, for long-wavelength disturbances, a vortex of core radius a with a particular distribution of vorticity can be converted to an equivalent vortex of core radius a_e with uniform vorticity. Knowing this latter radius, the cutoff distance δ is then deduced from the relation $\delta=(a_e/2)e^{1/4}$.[1,33,34] As mentioned in the previous section, the Lamb–Chaplygin vortex pair is well

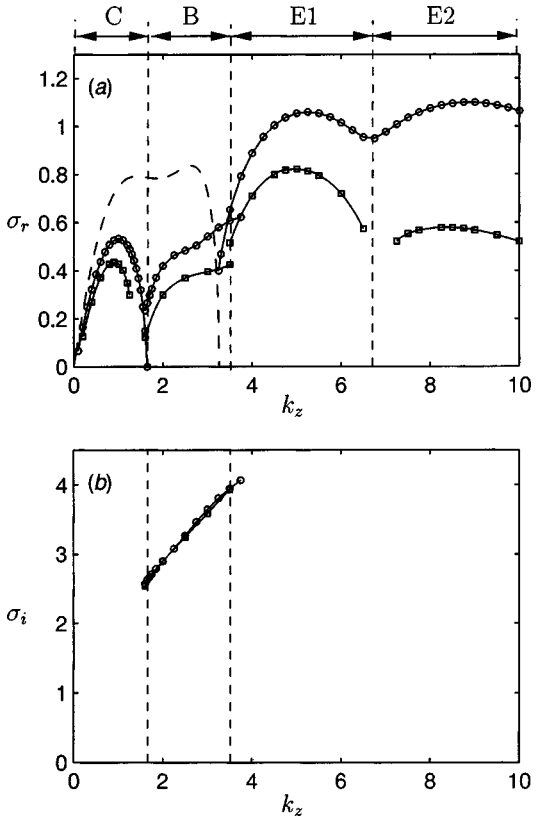

FIG. 5. Nondimensional growth rate σ_r (a) and frequency σ_i (b) of symmetric modes as a function of non-dimensional axial wave number k_z for $\mathrm{Re}=10^4$ (circle) and $\mathrm{Re}=400$ (square). Only nonzero frequencies σ_i are shown. The dashed line shows Crow's prediction for a pair of vortex filaments.

approximated by two Lamb–Oseen vortices with nondimensional core size $a=0.37$. Since the effective core size of a Lamb–Oseen vortex is known to be $a_e=1.36a$, this yields $a_e=0.5$. Alternatively, a_e can be also estimated from the results known for a vortex with the vorticity distribution $\omega_z=(r^{*2}-a_d^2)^2$. For such vortex, Widnall *et al.*[2] have obtained that $a_e=0.7a_d$. Therefore, taking a_d as the geometric mean between the semimajor and semiminor axes of the ellipse, i.e., $a_d=\sqrt{0.5}$, the same estimate for the effective core radius is obtained $a_e=0.5$. At low wave numbers, $k_z\leqslant 0.7$, Crow's theory agrees reasonably well with our numerical results [Fig. 5(a)]. The slight difference is probably due to the fact that the vortices in the Lamb–Chaplygin dipole are not well separated. At larger wave numbers, the long-wavelength Crow theory is no longer valid and departs widely from the numerically calculated stability curve.

In Fig. 6, we show a contour plot of the axial vorticity ω_z of the eigenmode for $k_z=1$ at which maximum amplification is achieved in the first instability band C. Note that ω_z is odd in y as implied by (11). If the perturbation axial vorticity were superposed to the axial vorticity of the basic state, it would be seen that this instability brings closer the two vortices of the pair and shifts them to the left, i.e., in the direction of propagation of the vortex pair. Conversely, if the sign of the perturbation is reversed (i.e., half a wavelength away), the two vortices move away from each other and are shifted to the right. Note that these perturbations do not distort the internal vortex structure in contrast with the short-wavelength antisymmetric instabilities described in the previous section. Such a scenario is consistent with the one described by Crow[1] in his Fig. 8.

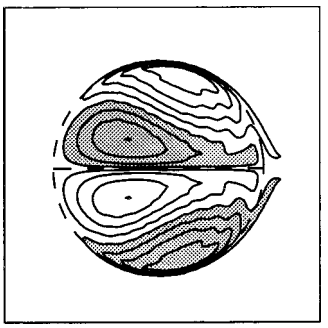

FIG. 6. Contours of axial vorticity in the horizontal plane of the Crow long-wavelength mode at $k_z=1$ for $\mathrm{Re}=10^4$. Same legend as in Fig. 3. Note that the small distortions seen on some contours disappear if a 512×512 resolution is used, but the growth rate changes by only 0.2%.

The second branch (B) of instability in Fig. 5(a) is oscillatory with a frequency σ_i shown in Fig. 5(b). The growth rate σ_r presents no maximum supposedly because this instability branch is hidden by more unstable branches C and $E1$ at low and high wave numbers. The axial vorticity ω_z at one phase of the oscillation cycle is shown in Fig. 7. Apart from the fact that the symmetry in y is reversed, this mode is similar to the antisymmetric oscillatory bulging instability mode described in the previous section [Fig. 3(a)]. However, the present symmetric mode is not observed to exist in the same wave number range as its antisymmetric counterpart. These differences probably result from the influence of the perturbation of each vortex on the other which are different in the antisymmetric and symmetric configurations. In particular, in the case of the symmetric mode, the two vortices of the pair bulge in phase and are likely to hinder each other. Note that a symmetric mode with a more complex radial structure similar to the antisymmetric mode of Fig. 3(b) has not been observed; the symmetric bulging eigenmode keeps the same structure over all wave numbers for which the oscillatory instability is the most dangerous.

The third and fourth instability branches labeled $E1$ and $E2$ in Fig. 5(a) are centered on the wave numbers $k_z=5.25$ and $k_z=8.75$ which are close to the wave numbers k_z

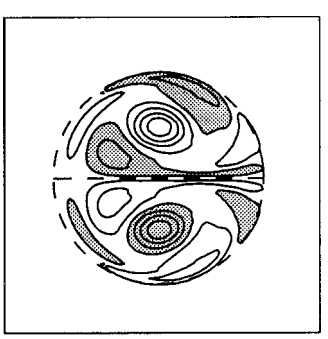

FIG. 7. Contours of axial vorticity of standing oscillatory symmetric mode in the horizontal plane at one phase of the oscillation cycle at $k_z=2.5$ for $\mathrm{Re}=10^4$. Same legend as in Fig. 3.

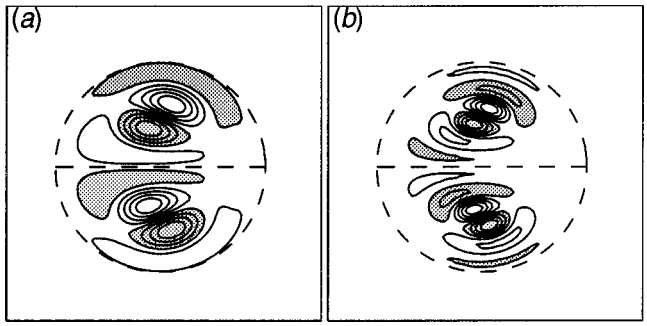

FIG. 8. Contours of axial vorticity of short-wavelength symmetric modes in the horizontal plane for the band $E1$ at $k_z=5.25$ (a) and for the band $E2$ at $k_z=8.75$ (b) for $\mathrm{Re}=10^4$. Same legend as in Fig. 3.

$=4.75$ and $k_z=8.5$ of maximum amplification of the short-wavelength antisymmetric modes for $\mathrm{Re}=10^4$ [Fig. 2(a)]. However, the associated maximum growth rates are lower ($\sigma_r=1.06$ and $\sigma_r=1.099$ for $\mathrm{Re}=10^4$) than those of the short-wavelength antisymmetric modes ($\sigma_r=1.26$ and $\sigma_r=1.21$, respectively). The axial vorticity corresponding to the $E1$ and $E2$ most amplified symmetric modes are displayed in Figs. 8(a)–8(b). These modes are very similar to their antisymmetric counterparts shown in Fig. 4 except that the symmetry by $y\rightarrow -y$ is reversed (in the terminology of Leweke and Williamson,[12] these instabilities would be therefore called ''anti-cooperative''). Like for the bulging instability, the occurrence of both symmetric and antisymmetric short-wavelength modes supports the idea that the elliptic instability occurs almost independently on each vortex of the pair. Yet, there exists a weak interaction between the perturbation of each vortex that causes the growth rate to be lower for the symmetric modes than for the antisymmetric ones.[12] In the first elliptic antisymmetric mode [Fig. 4(a)], the x-velocity which is induced by the perturbation field of the lower vortex on the upper vortex is in the same direction as the x-velocity induced by the perturbation of the upper vortex itself. By contrast, this induced velocity is opposite to the one locally induced in the symmetric mode [Fig. 8(a)]. There is therefore a kind of ''collaboration'' between perturbations of each vortex in the case of the antisymmetric mode whereas these perturbations do not cooperate in the symmetric mode.

IV. CONCLUSIONS

The three-dimensional stability of the Lamb–Chaplygin vortex pair appears to be quite rich. Because of the intrinsic symmetry of the basic state with respect to the middle plane between the two vortices, eigenmodes split into two independent classes, antisymmetric and symmetric modes. The most unstable eigenmodes of each of these two classes have been numerically determined as a function of the axial wave number at the Reynolds numbers $\mathrm{Re}=10^4$, approaching the inviscid limit and $\mathrm{Re}=400$, typical of experimental investigations. Elliptic and oscillatory bulging instabilities have been clearly identified, both with an antisymmetric and symmetric configurations. The antisymmetric mode is, however, always more unstable than its symmetric counterpart for both types of instability. A third type of instability is the long-wavelength Crow instability which is symmetric and has no antisymmetric counterpart. Of all these instabilities, the antisymmetric elliptic instability is the most unstable with a growth rate and a wavelength in very good agreement with recent experimental observations.[12]

On the practical side, we have shown that the elliptic instability theory of a single confined or unbounded vortex satisfactorily accounts for the short-wavelength instabilities of a real vortex pair. Crow's theory[1] for the long-wavelength symmetric instability works reasonably only at low wave number. A deficiency of the present study is that the effects of the distance between the two vortices have not been investigated since such distance is fixed in the Lamb–Chaplygin vortex pair. There exists a vortex pair family of solutions with vortices separated of an arbitrary distance.[36,37] However, the vortices have a uniform vorticity unlike real vortex pairs[12] and the Lamb–Chaplygin dipole. Recently, Sipp, Coppens, and Jacquin[38] have presented a stability analysis of vortex pairs with variable vortex separation, the basic state being obtained numerically.

On the theoretical side, an unexpected oscillatory bulging instability, similar to the one operating on Stuart vortices,[31] has been found. The evolution scenario of the eigenmodes' internal structure with additional radial nodes as the axial wave number increases is strikingly reminiscent of the elliptic instability one. In each vortex of the pair, the bulging eigenmode is dominated by $m=0$ and $|m|=2$ azimuthal modes. Therefore, just like the elliptic instability derives from a resonant interaction between the strain (whose intrinsic azimuthal wave number is $|m|=2$) (Refs. 2–4,10) and Kelvin waves with azimuthal wave number $m=+1$, $m=-1$ when they have the same frequency, this bulging instability could result from a resonant interaction of Kelvin waves with azimuthal wave number $m=0$ and $|m|=2$ with the strain.[3,18,31] Indeed, the instability mechanism discovered by Widnall *et al.*,[2] Moore and Saffman,[3] and Tsai and Widnall[4] is general and not restricted to $m=\pm 1$ Kelvin waves although this latter case has been studied in detail. Robinson and Saffman[5] discuss some of these possible other types of resonance. To further examine the plausibility of this hypothesis, we have calculated the frequency σ_i for Kelvin waves $m=0$ and $m=2$ on a Rankine vortex by solving numerically the dispersion relation (given for instance in Ref. 18). Figure 9 shows the frequency of the first four radial modes for both azimuthal wave numbers. It can be seen that there exist axial wave numbers for which Kelvin waves $m=0$ and $m=2$ have the same frequency. Interestingly, the two first crossing points (indicated by circles in Fig. 9) are at $k_z a_r=1.24$ and $k_z a_r=2.06$, that is to say, at axial wave numbers lower than those for which $m=\pm 1$ waves resonate ($k_z a_r=2.5$ and $k_z a_r=4.35$). Moreover the $m=0$ and $m=2$ waves cross at nonzero frequencies. Therefore, if an instability originates from these resonance points, it will be observed for axial wave number lower than those for which the elliptic instability occurs and would have an oscillatory behavior. This agrees qualitatively with the observed bulging instability. It remains however to determine whether or not the effect of strain is destabilizing near these crossing points.

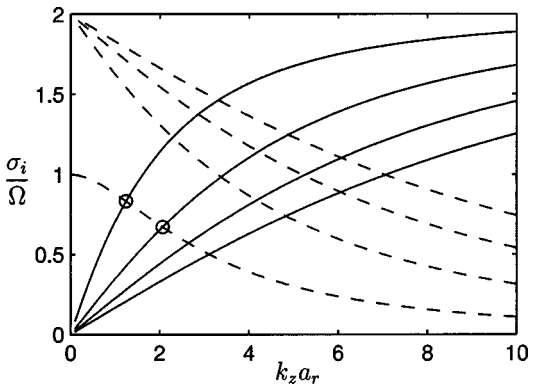

FIG. 9. Frequency σ_i of Kelvin waves with azimuthal wave number $m=0$ (solid lines) and $m=2$ (dashed lines) as a function of the axial wave number $k_z a_r$. Ω and a_r are the rotation rate and radius of the vortex.

This would require a quantitative mathematical treatment along the lines followed by Tsai and Widnall[4] and Moore and Saffman.[3]

ACKNOWLEDGMENTS

Special thanks go to J. Webert for his technical assistance. We acknowledge the Institut du Développement et des Ressources en Informatique Scientifique (IDRIS/CNRS) for computational facilities. We are grateful to O. Eiff for critically reading the manuscript. We would like to thank one of the referees for his constructive suggestions on the comparison with the experimental results of Leweke and Williamson.[12]

[1]S. C. Crow, ''Stability theory for a pair of trailing vortices,'' AIAA J. **8**, 2172 (1970).
[2]S. E. Widnall, D. B. Bliss, and C. Y. Tsai, ''The instability of short waves on a vortex ring,'' J. Fluid Mech. **66**, 35 (1974).
[3]D. W. Moore and P. G. Saffman, ''The instability of a straight vortex filament in a strain field,'' Proc. R. Soc. London, Ser. A **346**, 413 (1975).
[4]C. Y. Tsai and S. E. Widnall, ''The stability of short waves on a straight vortex filament in a weak externally imposed strain field,'' J. Fluid Mech. **73**, 721 (1976).
[5]A. C. Robinson and P. G. Saffman, ''Three-dimensional stability of an elliptical vortex in a straining field,'' J. Fluid Mech. **142**, 451 (1984).
[6]V. A. Vladimirov and K. I. Il'in, ''Three-dimensional instability of an elliptic Kirchhoff vortex,'' Mech. Zhid. Gaza **3**, 40 (1988).
[7]T. Miyazaki, T. Imai, and Y. Fukumuto, ''Three-dimensional instability of Kirchhoff's elliptic vortex,'' Phys. Fluids **7**, 195 (1995).
[8]R. T. Pierrehumbert, ''Universal short-wave instability of two-dimensional eddies in an inviscid fluid,'' Phys. Rev. Lett. **57**, 2157 (1986).
[9]B. J. Baily, ''Three-dimensional instability of elliptical flow,'' Phys. Rev. Lett. **57**, 2160 (1986).
[10]F. Waleffe, ''On the three-dimensional instability of strained vortices,'' Phys. Fluids A **2**, 76 (1990).
[11]P. J. Thomas and D. Auerbach, ''The observation of the simultaneous development of a long- and a short-wave instability mode on a vortex pair,'' J. Fluid Mech. **265**, 289 (1994).
[12]T. Leweke and C. H. K. Williamson, ''Cooperative elliptic instability of a vortex pair,'' J. Fluid Mech. **360**, 85 (1998).
[13]D. Delisi and R. Robins, ''Small-scale instability in trailing wake vortices in a stratified fluid,'' 28th A.I.A.A. Fluid Dyn. Conference 97-1784 (1997) (unpublished).
[14]T. Leweke and C. H. K. Williamson, ''Long-wavelength instability and reconnection of a vortex pair,'' in *IUTAM Symposium on Dynamics of Slender Vortices*, edited by E. Krause and K. Gersen (Kluwer Academic Publishers, 1998), p. 225.
[15]T. Sarpkaya, ''Trailing vortices in homogeneous and density-stratified media,'' J. Fluid Mech. **136**, 85 (1983).
[16]H. Lamb, *Hydrodynamics* (Cambridge University Press, Cambridge, 1932).
[17]G. K. Batchelor, *An Introduction to Fluid Dynamics* (Cambridge University Press, Cambridge, 1967).
[18]P. G. Saffman, *Vortex dynamics* (Cambridge University Press, Cambridge, 1992).
[19]V. V. Meleshko and G. J. F. van Heijst, ''On Chaplygin's investigations of two-dimensional vortex structures in an inviscid fluid,'' J. Fluid Mech. **272**, 157 (1994).
[20]Y. Couder and C. Basdevant, ''Experimental and numerical study of vortex couples in two-dimensional flows,'' J. Fluid Mech. **173**, 225 (1986).
[21]J. M. Nguyen Duc and J. Sommeria, ''Experimental characterization of steady two-dimensional vortex couples,'' J. Fluid Mech. **192**, 175 (1988).
[22]J. B. Flor and G. J. F. Van Heijst, ''An experimental study of dipolar vortex structures in a stratified fluid,'' J. Fluid Mech. **279**, 279 (1994).
[23]P. G. Drazin and W. H. Reid, *Hydrodynamic stability* (Cambridge University Press, Cambridge, 1981).
[24]R. T. Pierrehumbert and S. E. Widnall, ''The two- and three-dimensional instabilities of a spatially periodic shear layer,'' J. Fluid Mech. **114**, 59 (1982).
[25]I. Goldhirsch, S. A. Orszag, and B. K. Maulik, ''An efficient method for computing leading eigenvalues and eigenvectors of large asymmetric matrices,'' J. Sci. Comput. **2**, 33 (1987).
[26]C. K. Mamun and L. S. Tuckerman, ''Asymmetry and Hopf bifurcation in spherical Couette flow,'' Phys. Fluids **7**, 80 (1995).
[27]A. Vincent and M. Meneguzzi, ''The spatial structure and statistical properties of homogeneous turbulence,'' J. Fluid Mech. **225**, 1 (1991).
[28]P. Brancher ''Etude numérique des instabilités secondaires de jets,'' Ph.D. thesis, École Polytechnique, France, 1996.
[29]P. Brancher, J.-M. Chomaz, and P. Huerre, ''Direct numerical simulations of round jets: Vortex induction and side jets,'' Phys. Fluids **6**, 1768 (1994).
[30]I. Delbende, J.-M. Chomaz, and P. Huerre, ''Absolute/convective instabilities in the Batchelor vortex: A numerical study of the linear impulse response,'' J. Fluid Mech. **355**, 229 (1998).
[31]W. Schoppa, F. Hussain, and R. W. Metcalfe, ''A new mechanism of small-scale transition in a plane mixing layer: core dynamics of spanwise vortices,'' J. Fluid Mech. **298**, 23 (1995).
[32]P. Huerre and M. Rossi, ''Hydrodynamic instabilities in open flows,'' in *Hydrodynamics and Nonlinear Instabilities*, edited by C. Godrèche and P. Manneville (Cambridge University Press, Cambridge, 1998), p. 81.
[33]S. E. Widnall, D. B. Bliss, and A. Zalay, ''Theoretical and experimental study of the stability of a vortex pair,'' in *Aircraft Wake Turbulence and Its Detection*, edited by J. H Olsen, A. Goldburg, and M. Rogers (Plenum, New York, 1971), p. 305.
[34]S. E. Widnall, ''The structure and dynamics of vortex filaments,'' Annu. Rev. Fluid Mech. **7**, 141 (1975).
[35]R. Klein and O. M. Knio, ''Asymptotic vorticity structure and numerical simulation of slender vortex filaments,'' J. Fluid Mech. **284**, 275 (1995).
[36]G. S. Deem and N. J. Zabusky, ''Vortex waves: Stationary V-states, interactions, recurrence and breaking,'' Phys. Rev. Lett. **40**, 859 (1978).
[37]R. T. Pierrehumbert, ''A family of steady, translating vortex pairs with distributed vorticity,'' J. Fluid Mech. **99**, 129 (1980).
[38]D. Sipp, F. Coppens, and L. Jacquin, ''Theoretical and numerical analysis of vortex wake vortices,'' 3rd International workshop on vortex flows and related numerical methods, Toulouse, France, 1998 (unpublished).